Effects of Material Morphology on the Phototoxicity of Nano-TiO2 to Bacteria

ARTICLE *in* ENVIRONMENTAL SCIENCE & TECHNOLOGY · OCTOBER 2013

Impact Factor: 5.33 · DOI: 10.1021/es403079h · Source: PubMed

7 AUTHORS, INCLUDING:

Tiezheng Tong
Yale University
14 PUBLICATIONS **100** CITATIONS
SEE PROFILE

Jinsong Wu
Northwestern University
107 PUBLICATIONS **2,065** CITATIONS
SEE PROFILE

Binh Chu
University of Illinois at Chicago
14 PUBLICATIONS **372** CITATIONS
SEE PROFILE

John J Kelly
Loyola University Chicago
50 PUBLICATIONS **1,608** CITATIONS
SEE PROFILE

Environmental Science & Technology

Article

pubs.acs.org/est

Effects of Material Morphology on the Phototoxicity of Nano-TiO_2 to Bacteria

Tiezheng Tong,[†] Anas Shereef,[†] Jinsong Wu,[‡] Chu Thi Thanh Binh,[§] John J. Kelly,[§] Jean-François Gaillard,*[,†] and Kimberly A. Gray*[,†]

[†]Department of Civil and Environmental Engineering, Northwestern University, 2145 Sheridan Road, Evanston, Illinois 60208, United States

[‡]Department of Materials Science and Engineering, *NUANCE Center*, Northwestern University, Evanston, Illinois 60208, United States

[§]Department of Biology, Loyola University Chicago, 1032 West Sheridan Road, Chicago, Illinois 60660, United States

Supporting Information

ABSTRACT: Nanostructured titania (nano-TiO_2) is produced in diverse shapes, but it remains largely unknown how tuning the morphology of nano-TiO_2 may alter its toxicity. Herein, we show that material morphology plays a critical role in regulating the phototoxicity of nano-TiO_2 to bacteria. Low-dimensional nano-TiO_2, including nanotubes, nanorods, and nanosheets, were synthesized hydrothermally, and their effects on the bacterial viability of *Escherichia coli* and *Aeromonas hydrophila* were compared to spherical nanostructures (anatase nanospheres and P25). Results reveal that TiO_2 nanotubes and nanosheets are less phototoxic than their rod- and sphere-shape counterparts under simulated solar irradiation. None of the tested nano-TiO_2 shows toxicity in the dark. In contrast to their diminished phototoxicity, however, TiO_2 nanotubes and nanosheets exhibit comparable or even higher photoactivity than other nanostructures. Observations by scanning transmission electron microscopy suggest that material morphology influences nano-TiO_2 phototoxicity by governing how nano-TiO_2 particles align at the bacterial cell surface. Overall, when comparing materials with different morphologies and dimensionality, nano-TiO_2 phototoxicity is not a simple function of photocatalytic reactivity or ROS production. Instead, we propose that the evaluation of nano-TiO_2 phototoxicity encompasses a three-pronged approach, involving the intrinsic photoactivity, aggregation of nano-TiO_2, and the nano-TiO_2/bacteria surface interactions.

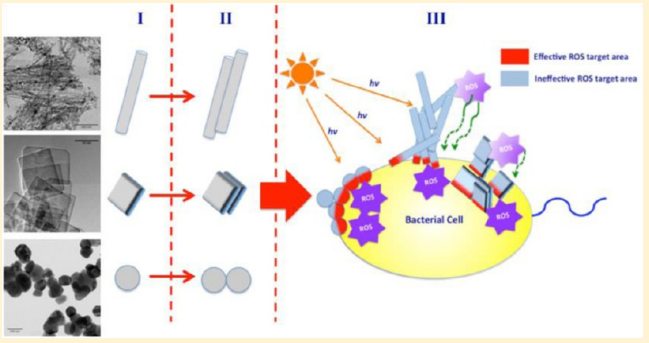

INTRODUCTION

The design of engineered nanomaterials (ENMs) with varying morphologies offers many opportunities to expand ENMs applications in the growing nanotechnology market. For instance, nanostructured titania (nano-TiO_2), a semiconductor with diverse applications ranging from sunscreens,[1] pigments,[2] and construction materials[3] to solar cells[4] and photocatalysts,[5] is commonly produced in spherical shapes (such as the most studied AEROXIDE P25). There are also low-dimensional TiO_2 nanostructures such as one-dimensional (1-D) nanotubes, nanorods, nanobelts, and nanowires[6,7] or two-dimensional (2-D) nanosheets[8] that have been recently developed and attracted considerable attention for their outstanding electronic, optical, and photocatalytic performance.[9−11] For example, TiO_2 nanosheets with preferential growth of highly reactive (001) facets display enhanced photoactivity in water splitting and organic pollutant degradation.[10,12] Also, vertically orientated TiO_2 nanotube arrays provide an optimal architecture for dye-sensitized solar cells.[13] Recently, Vijayan et al. demonstrated that calcination temperature can tune the morphology of hydrothermally synthesized 1-D TiO_2 nanostructures for improved photocatalytic activity.[14]

Despite promising new industrial applications, low-dimensional nano-TiO_2 materials may pose potential environmental and health risks due to the special properties promoted by their geometry. Only a few studies have probed the relationship between nanoparticle morphology and toxicity, but these investigations do provide evidence that morphology alters nanoparticle toxicity. Hamilton et al. found that longer TiO_2 nanobelts induced higher toxicity to both alveolar macrophages and mice than their shorter, spherical counterparts.[15] Pal et al. discovered that triangular-shape Ag nanoparticles displayed stronger antibacterial activity than sphere- and rod-shape nano-Ag.[16] Recently, Ji et al. reported that cerium oxide (CeO_2) nanorods/nanowires with higher aspect ratios caused more

Received: July 11, 2013
Revised: September 26, 2013
Accepted: October 1, 2013
Published: October 1, 2013

severe proinflammatory effects and cytotoxicity to human cells.[17] These pioneering studies indicate that morphology should be specifically considered in the risk assessment of nanomaterials.

However, those studies were conducted under nonilluminated conditions and focused primarily on eukaryotic cells, which suggest two questions about the potential ecotoxicity of nano-TiO_2. First, considering the significant structural and functional differences between prokaryotic bacteria and eukaryotic human/mammalian cells, the effect of morphology on bacterial toxicity of nano-TiO_2 is unknown. Second, electron−hole pairs generated under ultraband gap illumination react to form reactive oxygen species (ROS) that are highly deleterious to living cells.[18−21] Although the ecological and environmental implications of nano-TiO_2 phototoxicity have already been reported in the literature,[22−25] to the best of our knowledge there are no literature reports probing how material morphology affects nano-TiO_2 phototoxicity, particularly whether the enhanced photocatalytic performance of low-dimensional nano-TiO_2 amplifies phototoxic effects.

In the current study, we synthesized TiO_2 nanotubes, nanorods, and nanosheets using hydrothermal methods.[12,14] These low-dimensional TiO_2 nanostructures, along with two types of spherical nano-TiO_2, anatase nanospheres and AEROXIDE P25 (P25), allowed us to examine the effects of material morphology on nano-TiO_2 toxicity. The acute toxicity of nano-TiO_2 to *Escherichia coli* and *Aeromonas hydrophila* was assessed by measuring bacterial viability in a high-throughput screening (HTS) format in the presence/absence of simulated solar irradiation. *E. coli* is the most commonly used model bacterium in toxicity tests,[26,27] and *A. hydrophila* is a typical bacterial species found in natural aquatic environments.[28] We used Lake Michigan water for the exposure media, serving as a proxy of surface freshwaters. The phototoxicity of nano-TiO_2 was compared to the photocatalytic reactivity of nano-TiO_2 as measured by acetaldehyde photooxidation and hydroxyl radical (·OH) production. Furthermore, scanning transmission electron microscopy (STEM) was employed to image the interactions between nano-TiO_2 and bacterial cells. Our results delineate the relationship between morphology, photoactivity, and bacterial cytotoxicity of nano-TiO_2 and, therefore, reveal new insights into the mechanisms underlying nano-TiO_2 toxicity.

MATERIALS AND METHODS

Synthesis and Characterization of Nano-TiO_2 with Different Morphologies. TiO_2 nanotubes and nanorods were synthesized hydrothermally from an anatase powder precursor,[14] as detailed in the Supporting Information. Briefly, the anatase titania powder were treated with concentrated NaOH solution, and this alkali treatment resulted in the delamination of anatase titania powder to produce single-layer Na^+-intercalated TiO_2 sheets. Due to their large surface-to-volume ratio and high surface energy, these layered nanosheets spontaneously curled to form nanotubes. The formed nanotube was then washed with HCl and deionized water prior to calcination at different temperatures. The TiO_2 nanostructures produced at 400 °C maintained the tubular shape, while those produced at 600 °C collapsed to nanorods. The anatase precursor is spherical in shape and is named as "TiO_2 nanospheres", in order to differentiate it from P25 (Evonik Industries, Germany) that is also spherically shaped. TiO_2 nanosheets with a high fraction of (001) surfaces were synthesized hydrothermally using 20 mL of titanium butoxide (97%, Aldrich Chemicals, USA) and 3 mL of concentrated hydrofluoric acid (HF, 47%, Mallinckrodt Chemicals, USA), according to Han et al.[12] The above mixture was stirred magnetically for about 30 min and then heated at 200 °C for 24 h. The preferential interactions between fluoride and the (001) facets of TiO_2 crystal produce nanosheets with large fraction of highly reactive (001) facets.[10] The TiO_2 nanosheet precipitates were subsequently rinsed with 0.1 M NaOH solution to remove the excess, unreacted, and surface bound HF molecules and then with deionized water until a neutral pH of 6−7 was attained. For all the nano-TiO_2 samples, 1 g/L TiO_2 was prepared in Milli-Q water (Millipore, 18.2 MΩ·cm) as the stock solution, and a 1 h-sonication in ultrasonic bath (Health-Sonics, 110W, 42 kHz) was employed before diluting the stock solution to the desired concentrations for the toxicity tests.

The physicochemical properties of nano-TiO_2 samples were characterized by standard techniques. Specifically, the primary size and morphological features of nano-TiO_2 were observed using scanning electron microscopy (SEM, Hitachi S-4800-II) and transmission electron microscopy (TEM, Hitachi-2100). Powder X-ray diffraction (XRD) was used to determine the phase composition and crystallite size of each TiO_2 nanostructure. Dynamic light scattering (DLS) experiments were conducted to assess the sizes of nano-TiO_2 aggregates. The procedures for XRD and DLS are detailed elsewhere.[25] BET N_2 sorption measurements were performed with a Micromeritics ASAP 2010 unit to measure the nano-TiO_2 surface area, and a ZetaPALS zeta potential analyzer (Brookhaven Instruments) was used to measure the zeta potential and electrophoretic mobility of each nano-TiO_2 in the exposure medium.

Exposure Medium and Bacterial Cell Preparation. Lake Michigan water (LMW) was used as the exposure medium in all the solution-based toxicity and photoactivity tests. Untreated LMW was collected from the Evanston drinking water plant (Evanston, IL) and immediately transported to the laboratory where it was stored at 4 °C after filtration through a 0.2 μm pore-size membrane (NALGENE, Cat. 597-4520). The chemical composition of LMW is summarized in Table S1 (Supporting Information).

E. coli (ATCC 25922) and *A. hydrophila* (ATCC 23213) cells were cultured in Luria−Bertani (LB) broth at 25 °C overnight and harvested once they reached the mid-exponential phase. Then the bacterial cells were washed with 0.85% NaCl solution and with LMW twice in succession and finally resuspended in LMW. The final concentrations of *E. coli* and *A. hydrophila* used in the toxicity tests were about 5×10^7 CFU/mL and 3×10^7 CFU/mL, respectively, measured by direct plate counting.

High-Throughput Screening Analysis of Bacterial Viability. The bacterial cytotoxicity of nano-TiO_2 was assessed by the Live/Dead BacLight kit (Molecular Probes) that monitored cell membrane integrity as an indicator of bacterial viability. Two DNA dyes, SYTO9 and propidium iodide (PI), were utilized to differentiate viable and nonviable bacterial cells. Six concentrations of nano-TiO_2 (from 2.5 to 100 mg/L) were tested to obtain the dose−effects of nano-TiO_2 on bacteria. Although these concentrations are higher than previously predicted concentrations of nano-TiO_2 in aquatic environments,[29] they are necessary to reveal the acute bacteria toxicity of nano-TiO_2 and are within or lower than the concentration range used in many published reports.[30−32] The bacterial

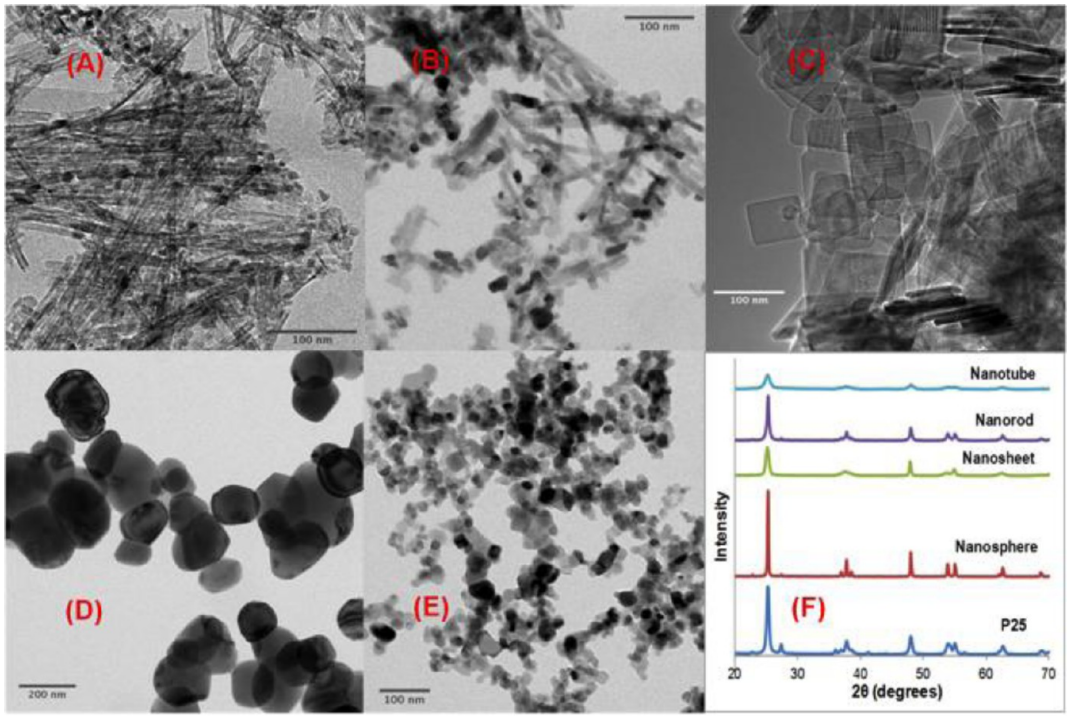

Figure 1. TEM micrographs of TiO_2 nanotubes (A), nanorods (B), nanosheets (C), nanospheres (D), and P25 (E); (F) XRD patterns of different TiO_2 nanostructures.

viability assay was conducted under both simulated solar irradiation and dark condition in a high-throughput screening format, as detailed in our previous work[25] as well as the Supporting Information. A xenon arc lamp (Model 6271, Newport) was used to provide simulated solar irradiation, and its intensity and spectrum were monitored by a calibrated spectrometer (EPP2000, StellarNet Inc., Figure S1). Since *A. hydrophila* was found to be more vulnerable to the simulated solar irradiation than *E. coli* (Figure S2), the exposure duration for *A. hydrophila* was shortened to 20 min, compared to that of 1 h for *E. coli*, thus minimizing the effect of the simulated solar irradiation alone on bacterial viability. Following the method of Jin et al.,[33] the percentage of viable bacteria for each nano-TiO_2 concentration was normalized to the percentage of viable cells in the TiO_2-free sample, in order to isolate the effect of nano-TiO_2 concentration on bacterial viability. At least three independent experiments were conducted to ensure experimental reproducibility. Furthermore, the potential interference of TiO_2 nanoparticles with this bacterial viability assay was investigated, following the "Minimum Exposure Time" (MET) method by Horst et al.[34] Our results show that this assay did not suffer from interference with TiO_2 nanoparticles (Figure S3 and detailed description in the Supporting Information).

Photocatalytic Activity and ·OH Production by Nano-TiO_2. The photocatalytic activity of nano-TiO_2 was first measured by monitoring the photooxidation of gas phase acetaldehyde over time.[35] In brief, 10 mg of nano-TiO_2 was placed in a photocatalytic system consisting of a closed square Teflon container with a quartz window. One mL of saturated vapor of acetaldehyde was introduced into the closed dark chamber and then allowed to equilibrate for 1 h. Then the photocatalytic reactions were carried out under full-spectra irradiation by a xenon arc lamp (Model 66902, Thermo Oriel). The intensity and spectra distribution of this xenon arc lamp are shown in Figure S1. As the photocatalytic reaction proceeded, the degradation of acetaldehyde was monitored every 20 min within 3 h using a gas chromatograph (HP 5890) equipped with a flame ionization detector. Three independent experiments were conducted to ensure experimental reproducibility.

The production of ·OH was measured by photooxidation of 3′-(p-hydroxyphenyl) fluorescein (HPF), as described by George et al.[36] HPF reacts specifically with ·OH to form fluorescent products without auto-oxidation in the presence of light illumination. In detail, nano-TiO_2 solutions (from 2.5 to 100 mg/L) were mixed with 10 μM of HPF in a 96-well microplate. Then the microplate was exposed to the same xenon arc lamp used in the toxicity tests for 10 min, followed by fluorescence detection (emission/excitation = 485/525 nm). The fluorescence intensity indicates the amount of ·OH generated by photoexcited nano-TiO_2. Three replicates were included within one microplate, and at least two independent microplates were analyzed to ensure the experimental reproducibility.

Scanning Transmission Electron Microscopy (STEM). STEM was used to visualize the interactions between nano-TiO_2 and the bacterial cells. Bacterial cells were prepared as described above and incubated with 50 mg/L of nano-TiO_2 in the dark for 30 min. Samples for STEM analysis were prepared by depositing a drop of bacteria-TiO_2 suspension onto a carbon-coated copper grid (Cat. 01820, Ted Pella, Inc., Formvar film removed). The edge of the grid was gently blotted with a filter paper followed by immediate cryofixation in liquid nitrogen to form vitrified ice/water. After that, the sample was transferred at cryogenic temperature into the microscope using a precooled cryosample holder. The stage was then warmed slowly from −170 °C while maintaining the vacuum to sublime the ice to the final temperature of −70 °C. Micrographs were acquired using an ultrahigh-resolution field emission scanning transmission electron microscope (Hitachi

Table 1. Physicochemical Characteristics of Six Nano-TiO_2 Tested in This Study

TiO_2 nanostructures	nanotubes	nanorods	nanosheets	nanospheres	P25
length, nm[a]	50−120	20−50	50−130	70−200	15−25
width, nm[a]	8−10	8−10	-	-	-
thickness, nm[a]	-	-	6−8	-	-
phase composition[b]	100% A[c]	98% A, 2% R	100% A	98% A, 2% R	84% A, 16% R
crystallite size[b], nm	10.1 ± 0.3	27.3 ± 0.8	16.8 ± 0.5	86.0 ± 1.8	22.5 ± 0.3
surface area,[d] m^2/g	245.1 ± 1.1	92.8 ± 0.5	118.5 ± 0.7	13.0 ± 0.1	74.3 ± 0.4
zeta potential, mV	−15.27 ± 0.97[e]	−13.16 ± 0.89	−17.20 ± 0.61	−18.75 ± 1.15	−14.40 ± 1.92
mobility, 10^{-8} $m^2/V{\cdot}s$	−1.19 ± 0.08	−1.03 ± 0.07	−1.34 ± 0.05	−1.46 ± 0.09	−1.12 ± 0.15

[a]From TEM. [b]From XRD. [c]A = anatase, R = rutile. [d]From BET analysis. [e]Standard deviation (n = 3).

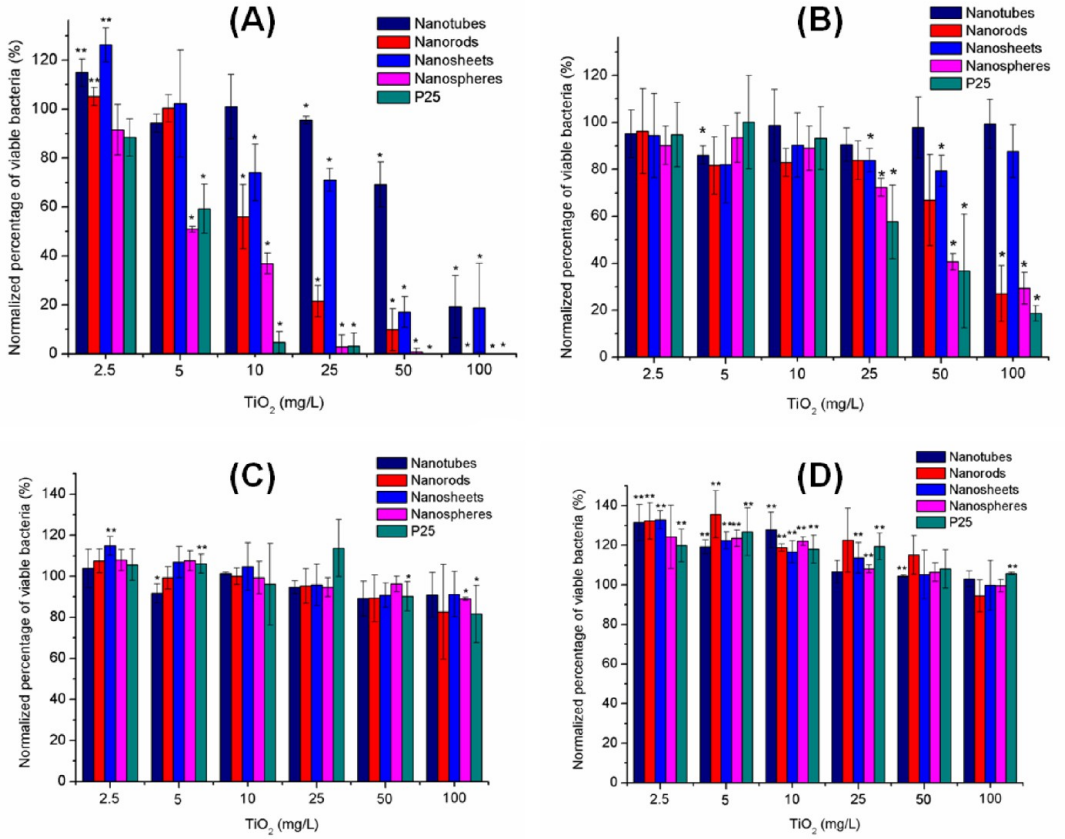

Figure 2. Bacterial viability of *E. coli* and *A. hydrophila* exposed to different nano-TiO_2. (A, B) *E. coli* (A) and *A. hydrophila* (B) under simulated solar irradiation. The exposure durations for *E. coli* and *A. hydrophila* were 1 h and 20 min, respectively. (C, D) *E. coli* (C) and *A. hydrophila* (D) in the dark for 1 h. One asterisk indicates a statistically significant decrease in bacterial viability ($p < 0.05$) compared to the TiO_2-free control, whereas two asterisks indicate an increase in bacterial viability ($p < 0.05$).

HD-2300A) operating at an accelerating voltage of 200 kV. Elemental compositions, elemental maps, and spectral line profiles of each sample were obtained using the dual energy dispersive spectroscopy (EDS) units (Thermo Scientific) operating at high sensitivity attached to the Hitachi HD-2300A STEM.

RESULTS AND DISCUSSION

Physicochemical Characterization and Aggregation Kinetics of Nano-TiO_2. Electron microscopy was used to define the primary size and morphology of each TiO_2 nanostructure (Figure S4 for SEM and Figure 1 for TEM). The anatase precursors of nanotubes and nanorods are roughly spherical with a primary size range of 70−200 nm (average of 130 nm, Figure 1D) and are referred to as "TiO_2 nanospheres". After the hydrothermal treatment, the TiO_2 nanostructures calcined at 400 °C exhibit a clear tubular morphology, with diameters of 8−10 nm and lengths of 50−120 nm (Figure 1A). At 600 °C the nanotubes collapse to form TiO_2 nanorods with similar diameters (8−10 nm) but shortened lengths (20−50 nm) (Figure 1B). The synthesized nanosheets display a well-defined rectangular outline (Figure 1C), having two-dimensions with side lengths of 50−130 nm and thickness of 6−8 nm. P25 is spherical with diameters of 15−25 nm (Figure 1E), consistent with literature reports.[23] XRD patterns (Figure 1F) show that most of the TiO_2 samples are predominantly anatase, except for P25 that contained ~16% rutile. The crystallite size of each nano-TiO_2 sample is also derived from the XRD patterns (Table 1), using the Scherrer equation on the anatase (101) plane diffraction peak. TiO_2 nanotubes and nanosheets

show the smallest crystallite sizes (10.1 and 16.8 nm, respectively), compared to P25 (22.5 nm), nanorods (27.3 nm), and nanospheres (86.0 nm). In addition, low-dimensional nano-TiO_2 display larger surface areas than spherical nano-TiO_2, as revealed by BET analysis: the surface areas of the nanotubes, nanorods, and nanosheets are 245.1, 92.8, and 118.5 m^2/g, respectively, in comparison to those of the nanospheres (13.0 m^2/g) and P25 (74.3 m^2/g).

In order to obtain toxicological data with better environmental relevance, the toxicity tests were conducted in LMW, and nano-TiO_2 aggregation was monitored by DLS (Figure S5). Due to the nonspherical morphology of TiO_2 nanotubes, nanorods, and nanosheets, the hydrodynamic diameters estimated by DLS were actually equivalent to the diameters of spherical particles with the same translational diffusion coefficients, as Ji et al. suggested.[17] All the nano-TiO_2 formed aggregates well beyond their original nanoscale in LMW, even at the onset of the experiment (at 0 min). This rapid aggregation is explained by ionic strength effects and decreased electrostatic repulsion in LMW, consistent with previous reports of metal oxide aggregation in natural water.[37,38] However, the nano-TiO_2 materials differed in their extent of aggregate growth. TiO_2 nanospheres showed the least extent of aggregation at both 10 and 50 mg/L, whereas TiO_2 nanorods, nanosheets, and P25 had similar aggregate sizes. Notably, TiO_2 nanotubes showed an extremely large aggregate size at 50 mg/L (7 μm on average after 0.5h-incubation in LMW), albeit with a high variation between replicate measurements. We attribute this phenomenon to the anisotropy and high aspect ratio of TiO_2 nanotubes, which gives very different diffusion coefficients associated with the translational motions parallel and perpendicular to the tube. This difference led to a large equivalent hydrodynamic diameter (mainly attributed to their length) and high variability between independent measurements. Moreover, although microsized aggregates measured by DLS are often reported in the literature,[23,37,39] they may not undergo Brownian motion on which DLS is based. Therefore, it must be noted that DLS does not measure the exact sizes of nano-TiO_2 aggregates. Instead, this technique only reflects the relative extent of aggregation by different TiO_2 nanostructures and, in particular, the unique aggregate structure formed by the nanotubes.

Cytotoxicity of Different TiO_2 Nanostructures to Bacteria. The BacLight bacterial viability assay was employed to evaluate the cytotoxicity of nano-TiO_2 to bacteria by monitoring membrane integrity, a well-accepted criterion for characterizing viable bacterial cells.[40,41] Figure 2A and B illustrates the bacterial viability of *E. coli* and *A. hydrophila* exposed to different TiO_2 nanostructures under simulated solar irradiation, respectively. Results of both bacteria show that low dimensional TiO_2 nanostructures, such as nanotubes and nanosheets, were significantly less phototoxic than their spherical counterparts, with the order of phototoxicity generally following P25 ≈ nanospheres > nanorods > nanosheets ≈ nanotubes. Compared to the TiO_2-free control, 25 mg/L of TiO_2 P25, nanospheres, and nanorods inactivated about 97%, 97%, and 78% of *E. coli* cells after 1 h-exposure, respectively. In contrast, only 4% and 29% of *E. coli* cells lost their viability when exposed to the same dose of TiO_2 nanotubes and nanosheets (Figure 2A). The corresponding IC_{50} (the TiO_2 concentration that results in 50% normalized bacterial viability) values were 5.9, 5.3, 11.5, 29.3, and 66.8 mg/L for P25, nanospheres, nanorods, nanosheets, and nanotubes, respectively (Figure S6). Similarly, 50 mg/L of TiO_2 P25, nanospheres, and nanorods led to *A. hydrophila* viability of 37%, 41%, and 67% after 20 min-exposure, compared to 80% and 98% viability at the same dose of nanosheets and nanotubes (Figure 2B). In the dark, however, negligible cytotoxicity to *E. coli* and *A. hydrophila* was observed for all the tested nano-TiO_2 (Figure 2C and D), indicating that the acute bacterial toxicity of nano-TiO_2 is predominantly due to their phototoxicity. These findings are consistent with those reported in many previous studies,[22,24,25,42] emphasizing the importance of illumination conditions in the risk assessment of nano-TiO_2. Interestingly, nano-TiO_2 exerted a stimulatory effect at low doses in the dark for *A. hydrophila* (Figure 2D), which we have shown was not caused by an interference of TiO_2 nanoparticles with the bacterial viability assay (Figure S3). The increase in relative bacterial viability may be due to a slight decrease in the *A. hydrophila* viability of the control sample (no TiO_2), whereas bacterial cells survived better or grew after nano-TiO_2 exposure (see Figures S7 and S8 for detailed explanation). Similar stimulatory effects have been reported for nano-TiO_2, fullerol, and nano-Ag in previous studies.[31,43,44] Hence, it may be a common phenomenon induced by a range of nanoparticles at sublethal doses or conditions, but its mechanism is not well understood at the present time and requires further study.

Our results demonstrate that material morphology has a marked influence on the bacterial cytotoxicity of nano-TiO_2, with low-dimensional TiO_2 nanostructures such as nanotubes and nanosheets, being less phototoxic than the spherical nanostructures. This finding, however, differs from both the Pal et al. study where nonspherical Ag nanoparticles are more toxic to bacteria[16] and other findings that nanoparticles with a higher aspect ratio cause more severe cytotoxicity to human/mammalian cells.[15,17] We propose that these inconsistencies reflect mechanistic differences between (I) phototoxicity and illumination-independent toxicity and (II) prokaryotic bacteria and eukaryotic cells' cytotoxic responses to nanoparticles. First, the toxicity of Ag nanoparticles is mainly due to Ag dissolution and the effects of free ions.[43] The strongest bactericidal effect observed with triangular nano-Ag is attributed to its highly reactive (111) facet with high atom density.[16] In contrast, the nano-TiO_2 is chemically stable, and its toxicity is predominantly caused by ROS generation with ultraband gap excitation.[18−21] Thus, material morphology plays different roles in regulating toxicity of nano-Ag and nano-TiO_2. Second, bacterial cells do not have the "macrophage-like" responses such as active engulfment of nanoparticles and production of proinflammatory mediators, both of which are responsible for nanoparticle toxicity to the human/mammalian cells typically used in toxicity tests.[17,45] Therefore, the influence of morphology on cellular uptake of nanoparticles does not contribute to regulating nano-TiO_2 toxicity in our study. We noted that Liu et al. reported that well-dispersed single-wall carbon nanotubes behaved as "nano-darts" to damage bacterial cells.[46] However, physical puncture is an illumination-independent mechanism and is inconsistent with the lack of toxic effects for all the nano-TiO_2 in the dark (Figure 2C, D). Furthermore, the aggregation of nano-TiO_2 in LMW undermines this potential "nano-dart" effect.

Photocatalytic Activity of Different TiO_2 Nanostructures. Since the phototoxicity of TiO_2 is mediated by photochemical events such as ROS photoproduction, the photocatalytic activities of different TiO_2 nanostructures were

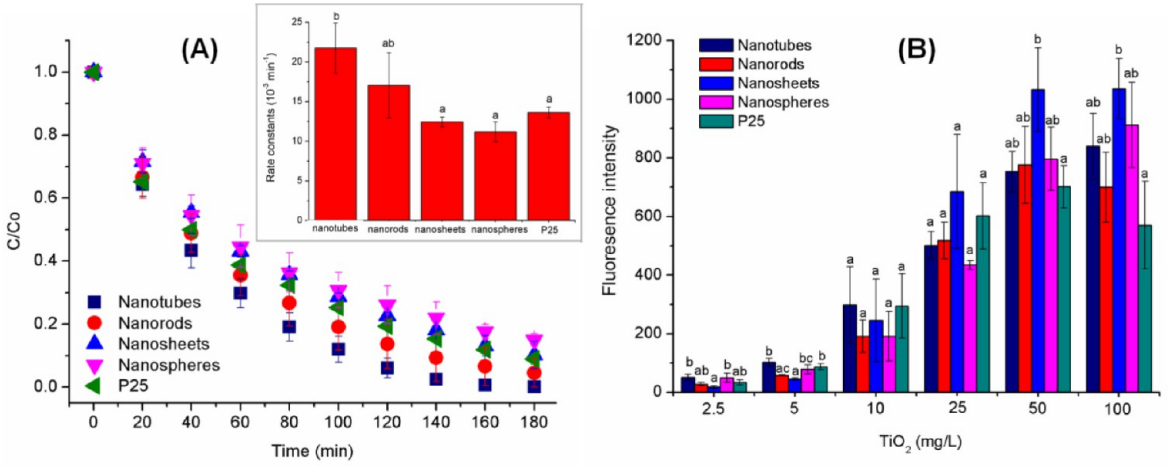

Figure 3. Photoactivity of different nano-TiO_2 under simulated solar irradiation. (A) Acetaldehyde photooxidation. The inset shows the rate constants according to the pseudo-first-order reaction. (B) ·OH production as indicated by HPF photooxidation. Different letters above the error bars indicate statistically significant differences between different TiO_2 nanostructures ($p < 0.05$) based on Tukey's HSD test.

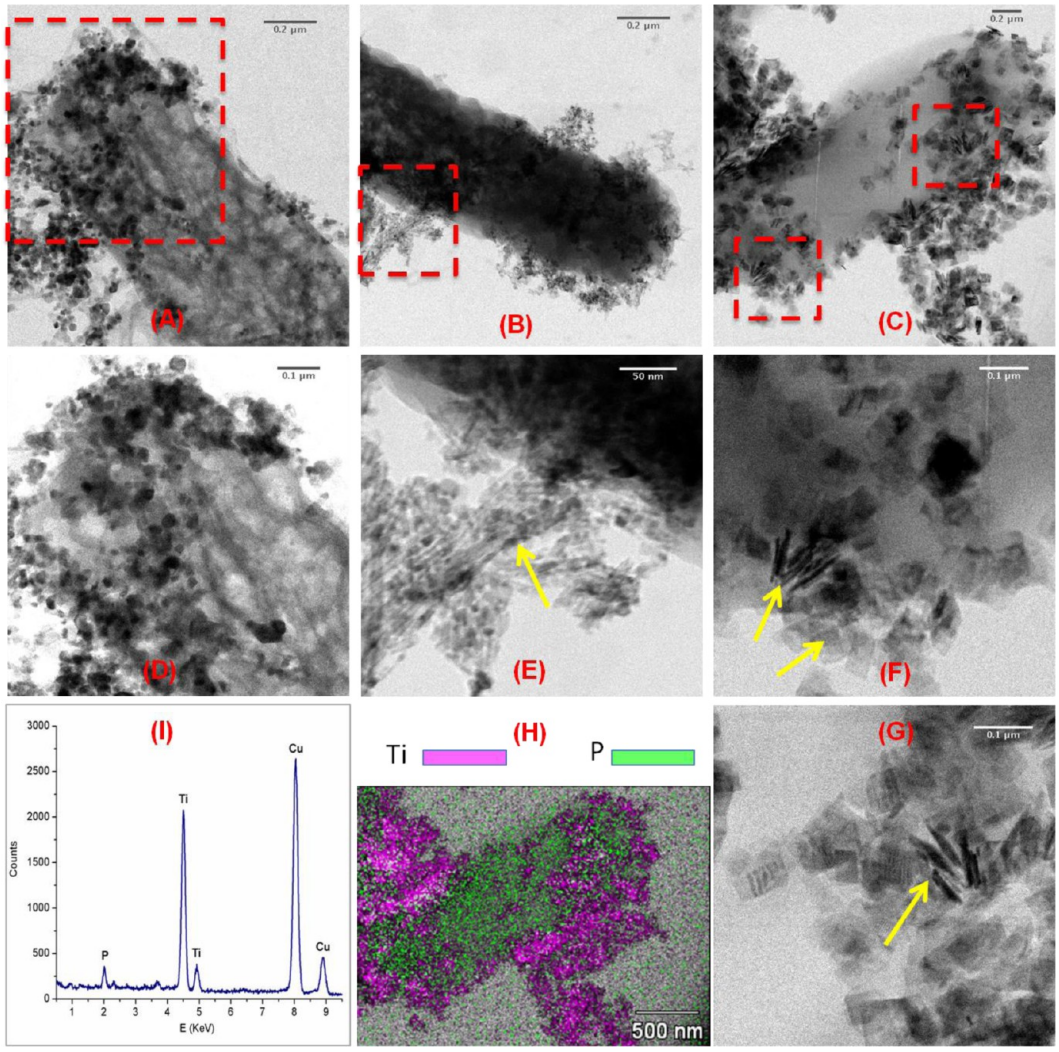

Figure 4. STEM and EDS analysis of the bacteria/nano-TiO_2 interactions. *E. coli* cells were exposed to 50 mg/L of TiO_2 P25 (A, D), nanotubes (B, E), and nanosheets (C, F, G) in the dark. Micrographs D, E, and F, G show higher magnification views of the areas indicated by the red dashed squares in A, B, and C, respectively. The yellow arrows in E, F, and G indicate nanotubes and nanosheets attaching to the bacterial cells only by their ends and edges, respectively. The elemental map obtained by EDS (H) confirms the location of the bacteria cell and TiO_2 nanoparticles (in part C). The elemental profile shown in I is obtained by scanning the entire area of H.

dx.doi.org/10.1021/es403079h | *Environ. Sci. Technol.* 2013, 47, 12486−12495

compared. Acetaldehyde photooxidation is a commonly used indicator for photocatalytic activity,[14,35,47,48] the pathway of which proceeds through radical oxidative reactions on the nano-TiO_2 surface.[49] Figure 3A illustrates the decay of acetaldehyde exposed to different nano-TiO_2 at the same mass loading (10 mg) under simulated solar irradiation. Following a pseudo-first-order reaction, the rate constants of acetaldehyde photooxidation were obtained (Figure 3A, inset). Results show that TiO_2 nanotubes and nanorods exhibited relatively higher acetaldehyde degradation rates (21.5×10^{-3} min^{-1} for nanotubes and 17.1×10^{-3} min^{-1} for nanorods) than the sphere-shape TiO_2 nanostructures (11.2×10^{-3} min^{-1} for nanospheres and 13.6×10^{-3} min^{-1} for P25) and TiO_2 nanosheets (12.4×10^{-3} min^{-1}), although the difference in the photoactivity between nanorods and other nanostructures was not statistically significant. Hence, in contrast to their diminished phototoxicity, the TiO_2 nanotubes and nanosheets displayed comparable or even higher photocatalytic reactivity than their rod- and sphere-shape counterparts.

In addition, photooxidation of HPF was used to compare the generation of ·OH by the TiO_2 nanostructures. In comparison to the gas-phase acetaldehyde photooxidation that tends to measure the intrinsic photocatalytic activity of nano-TiO_2, the HPF photooxidation was conducted in LMW and reflected the combination of solution effects and nano-TiO_2 aggregation. Figure 3B compares the extent of ·OH production by nano-TiO_2 at varying concentrations, as indicated by the measured fluorescence intensity. In general, ·OH production increased as the nano-TiO_2 concentration increased and was negatively correlated to the bacterial viability (Figure S9), indicating that ·OH radicals likely contribute to nano-TiO_2 phototoxicity. However, like acetaldehyde degradation, the monitoring of ·OH production failed to predict the order of bacterial phototoxicity of nano-TiO_2. At 10 and 25 mg/L of nano-TiO_2, for example, the ·OH yields were not statistically different among the nanostructures, although the nanospheres and P25 showed significantly higher phototoxicity to *E. coli* than the nanotubes and the nanosheets (Figure 2A). Similarly, in contrast to the phototoxicity trends (P25 > nanosheets), higher ·OH yields were measured for the nanosheets than P25 at 50 and 100 mg/L.

The photocatalytic reactivity of nano-TiO_2 is determined by the combined effects of surface area, surface energy, crystallinity, and charge separation efficiency.[12,14,50] The enhanced acetaldehyde decay by nanotubes and nanorods extends in part from their increased surface areas (Table 1). Using electron paramagnetic resonance spectroscopy Vijayan et al. showed that TiO_2 nanotubes and nanorods have distinct surface features that can lead to suppressed charge recombination and high photoactivity.[14] Therefore, the relative rates of the photocatalytic decay of acetaldehyde tend to reflect the effects of morphologically tuned nanoscale properties. Moreover, the slight discrepancy between the photoactivity measured by acetaldehyde degradation and HPF photooxidation can be explained by the aggregation of TiO_2 nanoparticles in LMW. The negative effects of particle aggregation on nano-TiO_2 photoactivity in solution have been reported by Jassby et al.[51] In contrast to previous work on simple TiO_2 nanoarchitectures (e.g., spheres),[25,52] neither photoactivity test, however, was predictive of the observed patterns of nano-TiO_2 phototoxicity. Thus, the phototoxicity of nano-TiO_2 is not a simple function of photocatalytic reactivity or ROS production when comparing materials with different morphologies and dimensionality, and additional factors influence the phototoxicity of nano-TiO_2.

STEM Observations of Nano-TiO_2/Bacteria Interactions. Recently, Herd et al. reported that silica nanoparticles with various geometries have different orientations at the macrophages cell surface, resulting in distinct nanoparticle uptake and toxicity mechanisms.[53] Similarly, morphology may determine the geometry and the alignment of the nano-TiO_2 particles at the bacterial cell surface and consequently affect their phototoxicity. Thus, we used STEM to observe bacteria/nano-TiO_2 interactions. We relied on a cryogenic preparation method that is the most likely to preserve the original arrangement between particles and bacteria in solution.[54] Figure 4 presents the micrographs of *E. coli* cells treated with 50 mg/L of TiO_2 P25 (Figure 4A, D), nanotubes (Figure 4B, E), and nanosheets (Figure 4C, F, G). Energy dispersive spectroscopy (EDS) was conducted to confirm the location of bacterial cells and nano-TiO_2 (Figure 4H, I). Additional micrographs including those on the nanorods- and nanospheres-bacteria interactions are presented in the Supporting Information (Figure S10).

The observations suggest that the alignment of the nano-TiO_2 particles/aggregates and their interactions with the bacterial cell surface are controlled by the nano-TiO_2 morphology. TiO_2 nanotubes aggregate into bundles, with many individual nanotubes aligning side-by-side (Figure 4E). Compared to end-to-end stacking, this bundled, parallel alignment results in smaller center-to-center distances between nanotubes and is favored by stronger van der Waals attractions.[17] Likewise, TiO_2 nanosheets were observed to stack and overlap each other (Figure 4C, F, G, and Figure S11). This dense packing of nanotubes and nanosheets significantly decreased their exposed surface area, diminishing contact with the bacterial surface. Moreover, the contact area was further minimized because of their orientation of attachment at the bacterial surface. Due to their anisotropy, the TiO_2 nanotube bundles and nanosheet stacks tended to be aligned at various angles to the bacterial surface rather than lying flat and were in contact with bacterial cell surface only at their ends or edges accounting for a small fraction of their total surface area (Figure 4E, F, G). In contrast, due to their spherical geometry and isotropy, P25 and nanospheres formed less compact aggregates, which do not show a particular orientation at the cell surface (Figure 4D, Figure S10E, F). Therefore, there was a greater degree of contact between spherical nano-TiO_2 and bacteria than nanotubes and nanosheets. For TiO_2 nanorods, their relatively low aspect ratios render them to behave more like P25 and nanospheres (Figure S10C, D).

We propose that limited contact areas with the bacterial surface explain the lower phototoxicity of TiO_2 nanotubes and nanosheets. The ROS generated by photoexcited nano-TiO_2 are known to mediate cell damage,[19,55] but the lifetimes of most ROS are very short (in the range of ns–μs [56]). The average diffusion distance of ·OH radicals is estimated to be only 2–6 nm[57–59] or 1–5 molecular diameters from their sites of formation.[56] Thus, the extent of nano-TiO_2 phototoxicity is determined not only by the total yield of photogenerated ROS but also by an "effective target area" near or on the bacterial surface from which the ROS molecules generated can reach and react with cellular components. Due to the combined effect of dense aggregation of TiO_2 nanotubes/nanosheets aligned with minimal contact at the bacterial surface, only a small proportion of the ROS radicals generated from those nanostructures

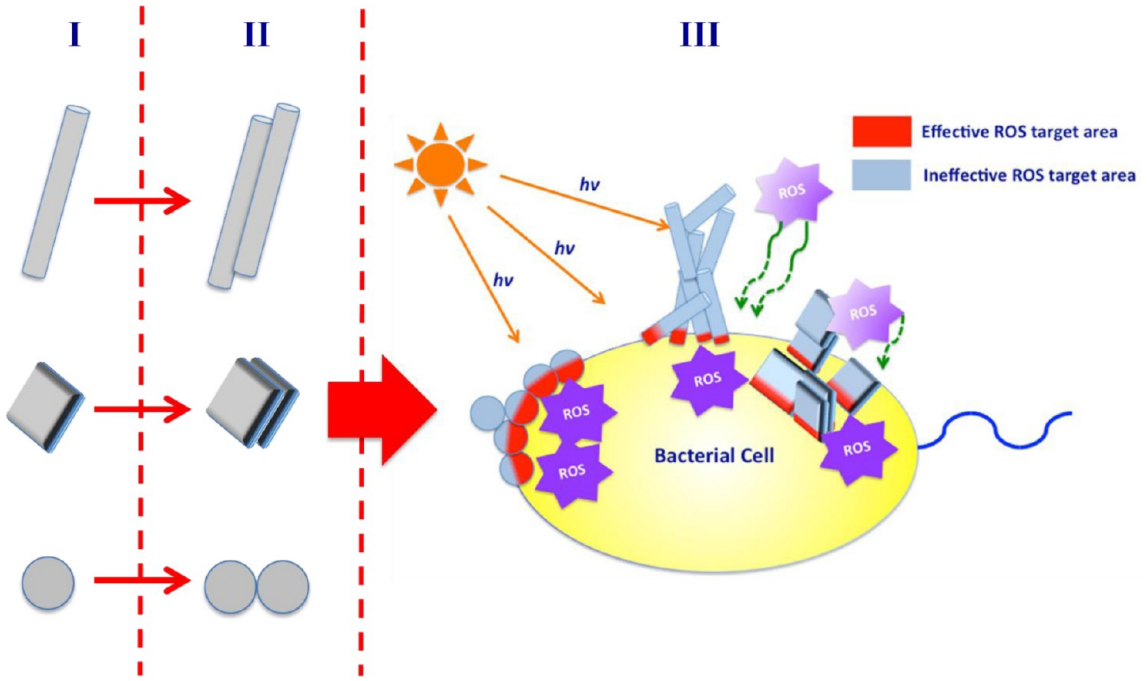

Figure 5. Schematic of the three-pronged approach to evaluate nano-TiO_2 phototoxicity.

diffuses to and reacts at the bacterial surface. Consequently the high levels of ROS production by nanotubes/nanosheets do not correlate with their low phototoxicity to bacteria. In contrast, a larger "effective ROS target area" is associated with P25, nanospheres, and nanorods and results in greater phototoxicity, even if their overall photoactivity may be less than nanotubes/nanosheets.

A Three-Pronged Approach To Evaluate Nano-TiO_2 Phototoxicity. In order to maximize the benefits of nano-TiO_2 in commercial use and minimize its environmental and health risks, an in-depth, mechanistic understanding of nano-TiO_2 toxicity is needed. We propose a three-pronged approach to evaluate the phototoxicity of nano-TiO_2 to bacteria comprehensively (Figure 5). Component I encompasses the intrinsic nanoscale photocatalytic properties of nano-TiO_2, which determines the potential of nano-TiO_2 in ROS production and bacterial photoinactivation. These properties are tuned by physical (e.g., shape) or chemical modifications that can enhance the photocatalytic reactivity of nano-TiO_2 and, consequently, their toxicity potential. Component II involves nano-TiO_2 aggregation in aqueous media that reduces the surface area and may increase charge carrier recombination.[51] The first two levels collectively define the ROS production by photoexcited nano-TiO_2. However, due to the short lifetime of ROS molecules, only those produced near/on the bacterial surface are ultimately able to induce phototoxicity. Gogniat et al.[60] showed that direct contact of TiO_2 particles with bacteria is required for their bacterial photoinactivation. Our results provide further evidence to support this conclusion and demonstrate the necessity of considering the geometry and alignment of nano-TiO_2 aggregates at the bacterial surface (Component III), in order to estimate the probability of ROS attack accurately. Accordingly, our study revises the simple predictive relationship between the photoactivity and the phototoxicity of nano-TiO_2, underscoring the complexity of predicting nano-TiO_2 ecotoxicity. The phototoxicity of nano-TiO_2 to bacteria is not determined by a single factor. Instead, multiple parameters, including photoactivity, material morphology, and aggregation, as well as bacteria/nano-TiO_2 contact, control the phototoxicity of nano-TiO_2 in synergetic ways. Our findings are valuable to both the intentional use of nano-TiO_2 as an oxidant, for instance, and its unintended environmental impacts in natural aquatic systems.

■ ASSOCIATED CONTENT

Supporting Information

Additional explanation, tables, and figures. This material is available free of charge via the Internet at http://pubs.acs.org.

■ AUTHOR INFORMATION

Corresponding Author

*Phone: (847)-467-4252. Fax: (847)-491-4011. E-mail: k-gray@northwestern.edu (K.A.G.). Phone: (847)-467-1376. Fax: (847)-491-4011. E-mail: jf-gaillard@northwestern.edu (J.-F.G.).

Notes

The authors declare no competing financial interest.

■ ACKNOWLEDGMENTS

This research was supported by the National Science Foundation (Grant No. CBET-1067751 to K.A.G. and J.-F.G. and Grant No. CBET-1067439 to J.J.K.). We thank Sara Fernandez Dunne, Corey Janczak, Jerry Carsello, Kevin Schwartzenberg, and Todd Eaton for their technical assistance and gratefully acknowledge the use of EPIC (NUANCE Center-Northwestern University), J. B. Cohen X-Ray Diffraction Facility and High-throughput Analysis Laboratory at Northwestern University.

■ REFERENCES

(1) Sadrieh, N.; Wokovich, A. M.; Gopee, N. V.; Zheng, J. W.; Haines, D.; Parmiter, D.; Siitonen, P. H.; Cozart, C. R.; Patri, A. K.; McNeil, S. E.; Howard, P. C.; Doub, W. H.; Buhse, L. F. Lack of significant dermal penetration of titanium dioxide from sunscreen

formulations containing nano- and submicron-size TiO_2 particles. *Toxicol. Sci.* **2010**, *115* (1), 156−166.
(2) Kaegi, R.; Ulrich, A.; Sinnet, B.; Vonbank, R.; Wichser, A.; Zuleeg, S.; Simmler, H.; Brunner, S.; Vonmont, H.; Burkhardt, M.; Boller, M. Synthetic TiO_2 nanoparticle emission from exterior facades into the aquatic environment. *Environ. Pollut.* **2008**, *156* (2), 233−239.
(3) Lee, J.; Mahendra, S.; Alvarez, P. J. J. Nanomaterials in the construction industry: A review of their applications and environmental health and safety considerations. *ACS Nano* **2010**, *4* (7), 3580−3590.
(4) Chen, X.; Mao, S. S. Titanium dioxide nanomaterials: Synthesis, properties, modifications, and applications. *Chem. Rev.* **2007**, *107* (7), 2891−2959.
(5) Li, G. H.; Ciston, S.; Saponjic, Z. V.; Chen, L.; Dimitrijevic, N. M.; Rajh, T.; Gray, K. A. Synthesizing mixed-phase TiO_2 nanocomposites using a hydrothermal method for photo-oxidation and photoreduction applications. *J. Catal.* **2008**, *253* (1), 105−110.
(6) Xia, Y. N.; Yang, P. D.; Sun, Y. G.; Wu, Y. Y.; Mayers, B.; Gates, B.; Yin, Y. D.; Kim, F.; Yan, Y. Q. One-dimensional nanostructures: Synthesis, characterization, and applications. *Adv. Mater.* **2003**, *15* (5), 353−389.
(7) Devan, R. S.; Patil, R. A.; Lin, J. H.; Ma, Y. R. One-dimensional metal-oxide nanostructures: Recent developments in synthesis, characterization, and applications. *Adv. Funct. Mater.* **2012**, *22* (16), 3326−3370.
(8) Liang, Y. T.; Vijayan, B. K.; Lyandres, O.; Gray, K. A.; Hersam, M. C. Effect of dimensionality on the photocatalytic behavior of carbon-titania nanosheet composites: Charge transfer at nanomaterial interfaces. *J Phys. Chem. Lett.* **2012**, *3* (13), 1760−1765.
(9) Schwartzenberg, K. C.; Gray, K. A. Nanostructured titania: The current and future promise of titania nanotubes. *Catal. Sci. Technol.* **2012**, *2* (8), 1617−1624.
(10) Liu, S. W.; Yu, J. G.; Jaroniec, M. Anatase TiO_2 with dominant high-energy {001} facets: Synthesis, properties, and applications. *Chem. Mater.* **2011**, *23* (18), 4085−4093.
(11) Shankar, K.; Basham, J. I.; Allam, N. K.; Varghese, O. K.; Mor, G. K.; Feng, X. J.; Paulose, M.; Seabold, J. A.; Choi, K. S.; Grimes, C. A. Recent advances in the use of TiO_2 nanotube and nanowire arrays for oxidative photoelectrochemistry. *J. Phys. Chem. C* **2009**, *113* (16), 6327−6359.
(12) Han, X. G.; Kuang, Q.; Jin, M. S.; Xie, Z. X.; Zheng, L. S. Synthesis of titania nanosheets with a high percentage of exposed (001) facets and related photocatalytic properties. *J. Am. Chem. Soc.* **2009**, *131* (9), 3152−3153.
(13) Shankar, K.; Bandara, J.; Paulose, M.; Wietasch, H.; Varghese, O. K.; Mor, G. K.; LaTempa, T. J.; Thelakkat, M.; Grimes, C. A. Highly efficient solar cells using TiO_2 nanotube arrays sensitized with a donor-antenna dye. *Nano Lett.* **2008**, *8* (6), 1654−1659.
(14) Vijayan, B.; Dimitrijevic, N. M.; Rajh, T.; Gray, K. Effect of calcination temperature on the photocatalytic reduction and oxidation processes of hydrothermally synthesized titania nanotubes. *J. Phys. Chem. C* **2010**, *114* (30), 12994−13002.
(15) Hamilton, R. F.; Wu, N. Q.; Porter, D.; Buford, M.; Wolfarth, M.; Holian, A. Particle length-dependent titanium dioxide nanomaterials toxicity and bioactivity. *Part. Fibre Toxicol.* **2009**, *6*, 35.
(16) Pal, S.; Tak, Y. K.; Song, J. M. Does the antibacterial activity of silver nanoparticles depend on the shape of the nanoparticle? A study of the gram-negative bacterium *Escherichia coli*. *Appl. Environ. Microb.* **2007**, *73* (6), 1712−1720.
(17) Ji, Z.; Wang, X.; Zhang, H.; Lin, S.; Meng, H.; Sun, B.; George, S.; Xia, T.; Nel, A. E.; Zink, J. I. Designed synthesis of CeO_2 nanorods and nanowires for studying toxicological effects of high aspect ratio nanomaterials. *ACS Nano* **2012**, *6* (6), 5366−5380.
(18) Hoffmann, M. R.; Martin, S. T.; Choi, W. Y.; Bahnemann, D. W. Environmental applications of semiconductor photocatalysis. *Chem. Rev.* **1995**, *95* (1), 69−96.
(19) Cho, M.; Chung, H. M.; Choi, W. Y.; Yoon, J. Y. Different inactivation behaviors of MS-2 phage and *Escherichia coli* in TiO_2 photocatalytic disinfection. *Appl. Environ. Microb.* **2005**, *71* (1), 270−275.
(20) Lipovsky, A.; Levitski, L.; Tzitrinovich, Z.; Gedanken, A.; Lubart, R. The different behavior of rutile and anatase nanoparticles in forming oxy radicals upon illumination with visible light: An EPR study. *Photochem. Photobiol.* **2012**, *88* (1), 14−20.
(21) Hirakawa, K.; Hirano, T. Singlet oxygen generation photocatalyzed by TiO_2 particles and its contribution to biomolecule damage. *Chem. Lett.* **2006**, *35* (8), 832−833.
(22) Bar-Ilan, O.; Chuang, C. C.; Schwahn, D. J.; Yang, S.; Joshi, S.; Pedersen, J.; Hammers, R. J.; Peterson, R. E.; Heideman, W. TiO_2 nanoparticle exposure and illumination during zebrafish development: Mortality at parts per billion concentrations. *Environ. Sci. Technol.* **2013**, *47*, 4726−4733.
(23) Battin, T. J.; Kammer, F. V. D.; Weilhartner, A.; Ottofuelling, S.; Hofmann, T. Nanostructured TiO_2: Transport behavior and effects on aquatic microbial communities under environmental conditions. *Environ. Sci. Technol.* **2009**, *43* (21), 8098−8104.
(24) Miller, R. J.; Bennett, S.; Keller, A. A.; Pease, S.; Lenihan, H. S. TiO_2 nanoparticles are phototoxic to marine phytoplankton. *PloS One* **2012**, *7* (1), e30321.
(25) Tong, T.; Binh, C. T. T.; Kelly, J. J.; Gaillard, J.-F.; Gray, K. A. Cytotoxicity of commercial nano-TiO_2 to *Escherichia coli* assessed by high-throughput screening: Effects of environmental factors. *Water Res.* **2013**, *47*, 2352−2362.
(26) Bowman, C. R.; Bailey, F. C.; Elrod-Erickson, M.; Neigh, A. M.; Otter, R. R. Effects of silver nanoparticles on zebrafish (*Danio rerio*) and *Escherichia coli* (ATCC 25922): A comparison of toxicity based on total surface area versus mass concentration of particles in a model eukaryotic and prokaryotic system. *Environ. Toxicol. Chem.* **2012**, *31* (8), 1793−1800.
(27) Cho, M.; Snow, S. D.; Hughes, J. B.; Kim, J. H. *Escherichia coli* inactivation by UVC-irradiated C_{60}: Kinetics and mechanisms. *Environ. Sci. Technol.* **2011**, *45* (22), 9627−9633.
(28) Hazen, T. C.; Fliermans, C. B.; Hirsch, R. P.; Esch, G. W. Prevalence and distribution of *Aeromonas Hydrophila* in the United States. *Appl. Environ. Microbiol.* **1978**, *36* (5), 731−738.
(29) Gottschalk, F.; Sonderer, T.; Scholz, R. W.; Nowack, B. Modeled environmental concentrations of engineered nanomaterials (TiO_2, ZnO, Ag, CNT, fullerenes) for different regions. *Environ. Sci. Technol.* **2009**, *43* (24), 9216−9222.
(30) Adams, L. K.; Lyon, D. Y.; Alvarez, P. J. J. Comparative eco-toxicity of nanoscale TiO_2, SiO_2, and ZnO water suspensions. *Water Res.* **2006**, *40* (19), 3527−3532.
(31) Simon-Deckers, A.; Loo, S.; Mayne-L'Hermite, M.; Herlin-Boime, N.; Menguy, N.; Reynaud, C.; Gouget, B.; Carriere, M. Size-, composition- and shape-dependent toxicological impact of metal oxide nanoparticles and carbon nanotubes toward bacteria. *Environ. Sci. Technol.* **2009**, *43* (21), 8423−8429.
(32) Metzler, D. M.; Li, M. H.; Erdem, A.; Huang, C. P. Responses of algae to photocatalytic nano-TiO_2 particles with an emphasis on the effect of particle size. *Chem. Eng. J.* **2011**, *170* (2−3), 538−546.
(33) Jin, X.; Li, M. H.; Wang, J. W.; Marambio-Jones, C.; Peng, F. B.; Huang, X. F.; Damoiseaux, R.; Hoek, E. M. V. High-throughput screening of silver nanoparticle stability and bacterial inactivation in aquatic media: Influence of specific ions. *Environ. Sci. Technol.* **2010**, *44* (19), 7321−7328.
(34) Horst, A. M.; Vukanti, R.; Priester, J. H.; Holden, P. A. An assessment of fluorescence- and absorbance-based assays to study metal-oxide nanoparticle ROS production and effects on bacterial membranes. *Small* **2012**, *9* (9−10), 1753−1764.
(35) Vijayan, B. K.; Dimitrijevic, N. M.; Wu, J. S.; Gray, K. A. The effects of Pt doping on the structure and visible light photoactivity of titania nanotubes. *J. Phys. Chem. C* **2010**, *114* (49), 21262−21269.
(36) George, S.; Pokhrel, S.; Ji, Z. X.; Henderson, B. L.; Xia, T.; Li, L. J.; Zink, J. I.; Nel, A. E.; Madler, L. Role of Fe doping in tuning the band gap of TiO_2 for the photo-oxidation-induced cytotoxicity paradigm. *J. Am. Chem. Soc.* **2011**, *133* (29), 11270−11278.

(37) French, R. A.; Jacobson, A. R.; Kim, B.; Isley, S. L.; Penn, R. L.; Baveye, P. C. Influence of ionic strength, pH, and cation valence on aggregation kinetics of titanium dioxide nanoparticles. *Environ. Sci. Technol.* **2009**, *43* (5), 1354−1359.
(38) Keller, A. A.; Wang, H. T.; Zhou, D. X.; Lenihan, H. S.; Cherr, G.; Cardinale, B. J.; Miller, R.; Ji, Z. X. Stability and aggregation of metal oxide nanoparticles in natural aqueous matrices. *Environ. Sci. Technol.* **2010**, *44* (6), 1962−1967.
(39) Chowdhury, I.; Duch, M. C.; Mansukhani, N. D.; Hersam, M. C.; Bouchard, D. Colloidal properties and stability of graphene oxide nanomaterials in the aquatic environment. *Environ. Sci. Technol.* **2013**, *47* (12), 6288−6296.
(40) Gregori, G.; Citterio, S.; Ghiani, A.; Labra, M.; Sgorbati, S.; Brown, S.; Denis, M. Resolution of viable and membrane-compromised bacteria in freshwater and marine waters based on analytical flow cytometry and nucleic acid double staining. *Appl. Environ. Microbiol.* **2001**, *67* (10), 4662−4670.
(41) Boulos, L.; Prevost, M.; Barbeau, B.; Coallier, J.; Desjardins, R. LIVE/DEAD (R) BacLight (TM): Application of a new rapid staining method for direct enumeration of viable and total bacteria in drinking water. *J. Microbiol. Methods* **1999**, *37* (1), 77−86.
(42) Yang, S. P.; Bar-Ilan, O.; Peterson, R. E.; Heideman, W.; Hamers, R. J.; Pedersen, J. A. Influence of humic acid on titanium dioxide nanoparticle toxicity to developing zebrafish. *Environ. Sci. Technol.* **2013**, *47* (9), 4718−4725.
(43) Xiu, Z. M.; Zhang, Q. B.; Puppala, H. L.; Colvin, V. L.; Alvarez, P. J. Negligible particle-specific antibacterial activity of silver nanoparticles. *Nano Lett.* **2012**, *12* (8), 4271−4275.
(44) Brunet, L.; Lyon, D. Y.; Hotze, E. M.; Alvarez, P. J. J.; Wiesner, M. R. Comparative photoactivity and antibacterial properties of C_{60} fullerenes and titanium dioxide nanoparticles. *Environ. Sci. Technol.* **2009**, *43* (12), 4355−4360.
(45) Nel, A. E.; Madler, L.; Velegol, D.; Xia, T.; Hoek, E. M. V.; Somasundaran, P.; Klaessig, F.; Castranova, V.; Thompson, M. Understanding biophysicochemical interactions at the nano-bio interface. *Nat. Mater.* **2009**, *8* (7), 543−557.
(46) Liu, S. B.; Wei, L.; Hao, L.; Fang, N.; Chang, M. W.; Xu, R.; Yang, Y. H.; Chen, Y. Sharper and faster "Nano Darts" kill more bacteria: A study of antibacterial activity of individually dispersed pristine single-walled carbon nanotube. *ACS Nano* **2009**, *3* (12), 3891−3902.
(47) Nishikiori, H.; Takei, M.; Oki, K.; Takano, S.; Tanaka, N.; Fujii, T. Photocatalytic activity of titania layer prepared by oxidizing titanium compounds on titanium plate surface. *Appl. Catal., B* **2012**, *127*, 227−233.
(48) Asahi, R.; Morikawa, T.; Ohwaki, T.; Aoki, K.; Taga, Y. Visible-light photocatalysis in nitrogen-doped titanium oxides. *Science* **2001**, *293* (5528), 269−271.
(49) Sopyan, I.; Watanabe, M.; Murasawa, S.; Hashimoto, K.; Fujishima, A. An efficient TiO_2 thin-film photocatalyst: Photocatalytic properties in gas-phase acetaldehyde degradation. *J. Photochem. Photobiol., A* **1996**, *98* (1−2), 79−86.
(50) Hurum, D. C.; Agrios, A. G.; Gray, K. A.; Rajh, T.; Thurnauer, M. C. Explaining the enhanced photocatalytic activity of Degussa P25 mixed-phase TiO_2 using EPR. *J. Phys. Chem. B* **2003**, *107* (19), 4545−4549.
(51) Jassby, D.; Budarz, J. F.; Wiesner, M. Impact of aggregate size and structure on the photocatalytic properties of TiO_2 and ZnO nanoparticles. *Environ. Sci. Technol.* **2012**, *46* (13), 6934−6941.
(52) Sayes, C. M.; Wahi, R.; Kurian, P. A.; Liu, Y. P.; West, J. L.; Ausman, K. D.; Warheit, D. B.; Colvin, V. L. Correlating nanoscale titania structure with toxicity: A cytotoxicity and inflammatory response study with human dermal fibroblasts and human lung epithelial cells. *Toxicol. Sci.* **2006**, *92* (1), 174−185.
(53) Herd, H.; Daum, N.; Jones, A. T.; Huwer, H.; Ghandehari, H.; Lehr, C. M. Nanoparticle geometry and surface orientation influence mode of cellular uptake. *ACS Nano* **2013**, *7* (3), 1961−1973.
(54) Mavrocordatos, D.; Perret, D.; Leppard, G. G. Strategies and Advances in the Characterisation of environmental colloids by electron microscopy. In *Environmental Colloids and Particles: Behaviour, Separation and Characterisation*; Wilkinson, K. J., Lead, J. R., Eds.; Wiley: 2007; Vol. *10*, pp 345−404.
(55) Li, Y.; Zhang, W.; Niu, J. F.; Chen, Y. S. Mechanism of photogenerated reactive oxygen species and correlation with the antibacterial properties of engineered metal-oxide nanoparticles. *ACS Nano* **2012**, *6* (6), 5164−5173.
(56) Pryor, W. A. Oxyradicals and related species - Their formation, lifetimes, and reactions. *Annu. Rev. Physiol.* **1986**, *48*, 657−667.
(57) Roots, R.; Okada, S. Estimation of life times and diffusion distances of radicals involved in X-ray-induced DNA strand breaks or killing of mammalian-cells. *Radiat. Res.* **1975**, *64* (2), 306−320.
(58) Bhattacharya, S. Action of X-irradiation on *E. coli*. *Radiat. Res.* **1961**, *14* (1), 50−55.
(59) Sanner, T.; Pihl, A. Significance and mechanism of indirect effect in bacterial cells. The relative protective effect of added compounds in *Escherichia coli* B, irradiated in liquid and in frozen suspension. *Radiat. Res.* **1969**, *37* (1), 216−227.
(60) Gogniat, G.; Thyssen, M.; Denis, M.; Pulgarin, C.; Dukan, S. The bactericidal effect of TiO_2 photocatalysis involves adsorption onto catalyst and the loss of membrane integrity. *FEMS Microbiol. Lett.* **2006**, *258* (1), 18−24.